

Texture-Induced Microwave Background Anisotropies

Julian Borrill^{1,2}, Edmund J. Copeland¹, Andrew R. Liddle¹,
Albert Stebbins³ and Shoba Veeraraghavan^{4,5}

¹*School of Mathematical and Physical Sciences,
University of Sussex,
Falmer, Brighton BN1 9QH, U. K.*

²*Blackett Laboratory*,
Imperial College of Science and Technology,
Prince Consort Road, London SW7 2BZ, U. K.*

³*NASA/Fermilab Astrophysics Center,
Fermi National Accelerator Laboratory,
Batavia, Illinois 60510, U. S. A.*

⁴*NASA Goddard Space Flight Center*,
Code 685, Greenbelt, MD 20771, U. S. A.*

⁵*Steward Observatory,
University of Arizona,
Tucson, Arizona 85721, U. S. A.*

Abstract

We use numerical simulations to calculate the cosmic microwave background anisotropy induced by the evolution of a global texture field, with special emphasis on individual textures. Both spherically symmetric and general configurations are analysed, and in the latter case we consider field configurations which exhibit unwinding events and also ones which do not. We compare the results given by evolving the field numerically under both the expanded core (XCORE) and non-linear sigma model (NLSM) approximations with the analytic predictions of the NLSM exact solution for a spherically symmetric self-similar (SSSS) unwinding. We find that the random unwinding configuration spots' typical peak height is 60-75% and angular size typically only 10% of those of the SSSS unwinding, and that random configurations without an unwinding event nonetheless may generate indistinguishable hot and cold spots. The influence of these results on analytic estimates of texture induced microwave anisotropies is examined, and comparison made with other numerical work.

PACS numbers: 98.80.Cq, 98.70.Vc

*Present address.



1 Introduction

The main rival to the inflationary cosmology [1] in explaining the origin of structure in the universe remains theories based on inhomogeneities formed at phase transitions. These inhomogeneities may be seeded by topologically stabilised objects such as cosmic strings [2], by the correlation of topologically trivial variations in the local direction of symmetry breaking, as with nontopological texture [3], or by a combination of the two, as with global strings [4], monopoles [5] or textures [3]. A proper assessment of the viability of such models requires a detailed understanding of their influence on the isotropy of the cosmic microwave background (CMB). In this paper we shall study some aspects of the CMB anisotropy produced by global textures.

Several authors have made studies of the predictions of the texture model for large scale structure [6] and CMB anisotropies [7, 8, 9, 10, 11]. The CMB predictions of textures can be compared with observations by the Differential Microwave Radiometer (DMR) on the Cosmic Background Explorer (COBE) satellite [12] to fix the one-parameter normalisation of the theory; however, the amplitude of density inhomogeneities then seems very small when normalized to COBE [9, 10]. Most CMB anisotropy calculations employ numerical simulations of the texture field evolution over a large volume of space, in some cases including the entire observable universe, and calculate the field's stress-energy tensor at each point at each time-step. Another approach involves calculating the anisotropy due to a single texture analytically and summing the result over an ensemble of textures with the appropriate number density and distribution.

A feature of defect field evolution peculiar to texture is that the field may order itself in two distinct ways. One mechanism is simply by smoothing its spatial gradients, a process which involves no topology change. The alternative is in a process known as 'unwinding'. During unwinding the field gradients near a point increase to such an extent that it becomes energetically possible for the field to pull itself off the vacuum manifold and over the symmetric-vacuum energy barrier, changing the local topological charge by unity. The only known non-trivial analytic solution of the texture field equations describes such an unwinding in the Non Linear Sigma Model (NLSM) approximation [7]. It is therefore standard to utilise this SSSS exact unwinding solution when describing textures analytically, including in the determination of CMB anisotropy detailed above. Despite breaking down at the unwinding event itself, where a singularity occurs and one must patch the ingoing to the outgoing solution, in general the NLSM approximation is an excellent one; however spherical symmetry and self-similarity are not good approximations to realistic configurations. We are therefore interested in how more general configurations compare with the SSSS case.

Recently, three of the present authors have published a two part numerical study of individual textures throughout which the NLSM approximation is lifted and the full field equations, including the potential term for the texture field, are used, giving non-singular evolution through the unwinding event. In the first part of the study [13] the assumption of spherical symmetry is retained but not that of self-similarity. In the second part [14] the spherically symmetric assumption is also dropped, allowing the study of texture unwinding events arising from randomly generated initial field configurations. One of the conclusions of the study is that the properties of the SSSS solution are not characteristic of those of more realistic random configurations (see also Ref. [15]). There are two aspects to this. The first, a problem with all spherically symmetric configurations, is that spherical symmetry sets up

very large scale correlations in the field, so that sections of the texture which are causally separated behave in a coherent way. The second is associated with the self-similarity; the initial field conditions also include a coherent velocity to keep it in the self-similar state, which provides a coherent ‘push’ on the texture towards unwinding. In the SSSS case this results in the texture unwinding as fast as is causally possible. Since the size of the CMB anisotropy is associated with the rate of change of the metric perturbations induced by the evolving field we might expect the typical anisotropy due to a more realistic texture configuration to have a less pronounced signature than that of the SSSS solution. In this paper we first calculate the anisotropy induced by a spherically symmetric but non-self-similar field configuration, and then those induced by general, randomly generated, configurations which have no particular symmetries or coherences. We thereby address the issue of how the CMB anisotropy patterns from realistic texture unwinding and non-unwinding configurations compare with that of the SSSS unwinding.

We wish to make a comparative study of CMB anisotropy produced by localized excitations of the texture field. Various processes can be important in determining the CMB anisotropy; e.g. Thomson scattering may or may not be important depending on whether the excitation is in front of or on the surface of last scattering, cosmological expansion can be more or less important depending on whether the coherence length of the texture excitation is large or small compared to the cosmological horizon, and finally various geometrical and physical effects are more or less important depending whether the excitation subtends a large or small angle on the sky. Since we are interested in a comparison of the different texture configurations and since the processes mentioned probably affect the different texture configurations in a similar way we feel it is reasonable to ignore all of these effects and to compare the CMB anisotropy for the texture excitations in the simplest possible environment. Here we will compare temperature patterns for texture excitations in Minkowski space. This is the appropriate limit if the texture excitations subtend a small angle, are well in front of the surface of last scattering and are much smaller than the horizon when we see them. This is independent of the redshift at which we see them.

An important consideration in computing any effect of textures in a cosmological setting involves determining appropriate initial conditions for both the texture fields and the matter fields. Energy and momentum are always locally conserved, so that the energy overdensity corresponding to the presence of a topological defect is locally compensated by an energy underdensity in the other fields [16]. Naïvely we might assume that compensation, by restoring the initial homogeneity of the total energy density, would automatically reduce the CMB anisotropy generated by a particular defect field configuration. However, as two of the present authors have shown [17], in many cases the compensating perturbations will increase and not decrease both the density perturbation and CMB anisotropy. Whether or not compensation will decrease or increase the CMB anisotropy for realistic texture configurations is not clear; however, the analytic work just cited suggests that we should expect no strong cancellation of CMB anisotropies due to compensation.

2 Texture Field Evolution

The central problem in numerical studies of texture evolution is that the ratio of the two fundamental length scales — the macrophysical field correlation length and the microphysical field width — is so large that it is impossible to resolve them on the simulation lattice

simultaneously. We therefore have to adopt one of two approximations, either massively enlarging the field width (the XCORE approximation) or shrinking it to zero (the NLSM approximation). If these results are to be taken seriously, it is crucial that these two different approximation methods give comparable results, and we shall see that this is indeed the case. A more detailed comparison and critique of these two approaches is given separately by one of us [18].

We work throughout in flat space with the texture field normalised such that the vacuum manifold is the 3-sphere $|\Phi| = 1$, so the potential is given by $V(\Phi) = V_0(\Phi^2 - 1)^2$. Discretising the equations of motion in both space and time then yields equations for $\Phi_{i,n}$ (where i-indices are spatial and n-indices temporal), giving the field at points separated by the grid-spacing δx and by the time step δt .

2.1 The XCORE Approximation

In flat space the equation of motion of the texture field Φ is

$$\ddot{\Phi} - \nabla^2 \Phi = -4V_0(\Phi^2 - 1)\Phi \quad (1)$$

Given the field at some time t and its velocity at time $(t - \delta t)/2$ these may now be discretised to second order using a standard staggered leapfrog approach [19], giving

$$\begin{aligned} \dot{\Phi}_{i,n+1/2} &= \dot{\Phi}_{i,n-1/2} + \left(\nabla^2 \Phi_{i,n} - 4V_0(\Phi_{i,n}^2 - 1)\Phi_{i,n} \right) \delta t \\ \Phi_{i,n+1} &= \Phi_{i,n} + \dot{\Phi}_{i,n+1/2} \delta t \end{aligned} \quad (2)$$

In order to be able to resolve the texture's core the field width must be unrealistically large, equivalent to making the mass of the radial mode unrealistically small. This approach was introduced for domain wall simulations in Ref. [20], and for texture simulations in Ref. [21]. Care must be taken to ensure that this approximation does not qualitatively affect the field's evolution, with the degree of the approximation being characterised by the ratio of the field width to its correlation length. We therefore work with an oversized field width

$$W_0 \equiv m_\Phi^{-1} = 1/\sqrt{8V_0} = 0.25 \delta x \quad (3)$$

on a grid with 96^3 points. We employ the catalogue of unwinding and non-unwinding random initial configurations developed in Ref. [14]; the initial configurations are set by randomly assigning field values on the manifold on a 3×3 grid, and interpolating between them (accounting for periodic boundary conditions) onto the 96^3 grid. The initial velocities are set to zero. A crude measure of the correlation length is therefore the separation of the uncorrelated points, and this value is large enough compared to the field width to be known not to qualitatively distort the field's evolution [22]. Having 27 independent correlation volumes of the field gives a reasonable chance, about 4%, of obtaining a texture unwinding in a simulation.

In so far as we can take the distance of 32 grid points between the randomly selected points to represent the correlation length, this provides an estimate of the initial 'horizon radius' in the simulations¹, which we note is considerably larger in grid units than in other

¹We are treading in dangerous waters here by mentioning horizon sizes whilst carrying out simulations in flat space. In expanding universes the horizon size is closely connected to the Hubble length, whereas here we intend the term to indicate the distance light can have travelled between some conceptual initial time when the correlation length approached zero and the time the simulation actually started, motivated by the knowledge that the texture field correlations grow at or close to the speed of light.

simulations, e. g. Refs. [10, 11]. The simulations are run for a maximum time of 48 grid units (though of course the actual number of time steps is much greater); further forward evolution endangers problems with the periodic boundary conditions.

For comparison we also consider a spherically symmetric non-self-similar initial configuration of the form

$$\Phi(r, \theta, \psi) = (\cos \chi(r), \sin \chi(r) \cos \theta, \sin \chi(r) \sin \theta \cos \psi, \sin \chi(r) \sin \theta \sin \psi) \quad (4)$$

$$\dot{\Phi} = 0 \quad (5)$$

with

$$\chi(r) = \pi(1 - e^{-r/r_0}) \quad (6)$$

and take $r_0 = 18 \delta x$ to satisfy the lattice resolution constraints.

2.2 The NLSM Approximation

In the NLSM approximation, the flat space equations of motion of the texture field become

$$\ddot{\Phi} - \nabla^2 \Phi = -(\dot{\Phi}^2 - \nabla \Phi^2) \Phi \quad (7)$$

Given the field at times t and $t - \delta t$ the equations of motion may be discretised to second order to give

$$\Phi_{i,n+1} = 2\Phi_{i,n} - \Phi_{i,n-1} + \nabla^2 \Phi_{i,n} \delta t^2 - (\dot{\Phi}_{i,n}^2 - \nabla \Phi_{i,n}^2) \delta t^2 \Phi_{i,n} \quad (8)$$

Following Ref. [10], we write this in the form

$$\Phi_{i,n+1} = \delta \Phi_{i,n} + \lambda \Phi_{i,n} \quad (9)$$

with

$$\begin{aligned} \delta \Phi_{i,n} &= \Phi_{i,n} - \Phi_{i,n-1} + \nabla^2 \Phi_{i,n} \delta t^2 \\ \lambda &= 1 - (\dot{\Phi}_{i,n}^2 - \nabla \Phi_{i,n}^2) \delta t^2 \end{aligned} \quad (10)$$

we can use the constraint $|\Phi_{i,n+1}| = 1$ to solve for λ , giving

$$\lambda = -\delta \Phi_{i,n} \cdot \Phi_{i,n} \pm \sqrt{1 - \delta \Phi_{i,n}^2 + (\Phi_{i,n} \cdot \delta \Phi_{i,n})^2} \quad (11)$$

Since $\delta \Phi_{i,n}$ is small

$$\Phi_{i,n+1} \sim \begin{cases} +\Phi_{i,n} & \text{taking the positive root in } \lambda \\ -\Phi_{i,n} & \text{taking the negative root in } \lambda \end{cases} \quad (12)$$

The choice of the negative root in the evaluation of λ is therefore equivalent to explicitly introducing an unwinding event at grid position i at time-step n . Since the NLSM approximation breaks down at unwindings, this provides a means of re-introducing them. However although this explicit re-introduction may be necessary for spherically symmetric configurations, whose unwinding sites can be predetermined and made to lie exactly on a gridpoint, for general field configurations unwindings occur implicitly, off the grid, and we should always take the positive root in λ . Indeed to do otherwise [10, 11] is not only unnecessary but also

incorrect since under the NLSM approximation *only* at the unwinding site itself should the field ever leave the vacuum manifold [18].

We can now take the same set of initial field configurations as in the XCORE runs, with identical simulation parameters, but now evolved via Eq. (9). For the spherically symmetric configuration, the unwinding occurs at a grid point and is explicitly introduced by taking the negative root in Eq. (11) when the field within one grid spacing of the unwinding site covers more than half of the vacuum manifold.

3 The CMB Anisotropy

3.1 Analytic Formalism

The evolving texture field will produce an inhomogeneous time-varying gravitational field. Photons travelling along different trajectories will gain or lose different amounts of energy in the time varying field which will thus result in different shifts in temperature of the CMB photons in different directions on the sky. For the weak fields produced by textures the temperature shifts are given by the Sachs-Wolfe integral [23]. The Sachs-Wolfe integral may be re-expressed as an integral over the stress-energy distribution which produces the gravitational fields. This last integral was examined in Ref. [24] for sources which are far from the observer and subtend small angles in flat space, and re-examined by Hindmarsh [25] in a rather clever and simple way which also applies to gravitational lensing. Extensions to large angles are given in Ref. [26] for flat space and in Ref. [27] for a matter-dominated FRW cosmology. Here we use the small-angle large-distance approximation in flat space. In this case the temperature pattern we see depends only on the stress-energy on the past light cone of the observer.

In the small-angle large-distance approximation the photons we see at one instant were approximately in a plane when they passed by the object we are viewing. We may thus label the temperature pattern by a 2-dimensional vector, \mathbf{x}_\perp , which is perpendicular to the direction \hat{n} in which we are looking. The congruence of photons may thus be approximated as $\mathbf{x}_\gamma(t) = \mathbf{x}_\perp - \hat{n}(t - t_i)$ where t_i is the impact time, so this plane passes by the observers at the time of observation. With this notation the temperature pattern is given by [26, 25]

$$\nabla_\perp^2 \frac{\Delta T}{T}(\mathbf{x}_\perp) = -8\pi G \nabla_\perp \cdot \mathbf{U}(\mathbf{x}_\perp) \quad (13)$$

where the 2-dimensional vector \mathbf{U} is (i, j, k, \dots are spatial indices)

$$U_i(\mathbf{x}_\perp) = -(\delta_i^j - \hat{n}_i \hat{n}^j) \int_{-\infty}^{\infty} (\Theta_{0j}(t, \mathbf{x}_\gamma(t)) - \hat{n}^k \Theta_{jk}(t, \mathbf{x}_\gamma(t))) dt \quad (14)$$

and $\Theta_{\mu\nu}(t, \mathbf{x})$ is the stress-energy tensor. Note that Eq. (13) only determines the temperature pattern up to an arbitrary function satisfying $\nabla_\perp^2 \phi = 0$. However setting zero boundary conditions at infinity determines the function uniquely, while the periodic boundary conditions that we shall use determine ϕ up to a constant. This constant is chosen so that the mean anisotropy is zero. The texture stress-energy tensor is

$$\Theta_{\alpha\beta} = \partial_\alpha \Phi \partial_\beta \Phi - g_{\alpha\beta} \mathcal{L} \quad (15)$$

and taking the line of sight to be $\hat{n} = (-1, 0, 0)$, Eq. (14) becomes

$$U_i(\mathbf{x}_\perp^\perp) = - \int_{-\infty}^{\infty} (\partial_0 \Phi + \partial_1 \Phi) \partial_i \Phi dt \quad (16)$$

for $i = 2, 3$. Given a field configuration and its initial distribution, Eqs. (14) and (16) determine the anisotropy completely.

There is an analytic solution to the field equations in the NLSM which describes an unwinding knot. The field configuration is spherically symmetric and remains on the vacuum manifold at all times. In spherical polar coordinates (r, θ, ϕ) ,

$$\Phi = (\cos \chi(r, t), \sin \chi(r, t) \cos \theta, \sin \chi(r, t) \sin \theta \cos \psi, \sin \chi(r, t) \sin \theta \sin \psi) \quad (17)$$

has only one degree of freedom, $\chi(r, t)$, remaining, and any non-singular configuration has $\chi(0, t) = 0$ or π . In this form the SSSS solution is

$$\chi(t, r) = \begin{cases} 2 \tan^{-1}(-r/t) & t < 0 \\ 2 \tan^{-1}(t/r) + \pi & 0 < t < r \\ 2 \tan^{-1}(r/t) + \pi & 0 < r < t \end{cases} \quad (18)$$

At the origin $\chi(0, t)$ jumps discontinuously from 0 to π at the unwinding at $t = 0$, and the outgoing solution has a gradient discontinuity at $r = t$ (though the stress-energy tensor remains smooth). Applying Eq. (13) to the SSSS solution one reproduces the result of Ref. [7], i.e.

$$\frac{\Delta T}{T} = \frac{t_i}{\sqrt{2|\mathbf{x}_\perp|^2 + t_i^2}} \epsilon \quad (19)$$

where $\epsilon = 8\pi^2 G \Phi_0^2$, $|\mathbf{x}_\perp|$ gives the impact parameter of the photon from the texture centre, and t_i gives the time that the photon sheet passes through the centre. The pattern is a cold spot of depth $-\epsilon$ if the photons pass the centre before unwinding ($t_i < 0$) and a hot spot of height $+\epsilon$ if the photons pass after unwinding ($t_i > 0$). The Full Width Half Maximum (FWHM) of the hot/cold spot, that is, the diameter of the circular ring centered on the spot, along which the temperature is half the central value, is $\sqrt{6}|t_i|$ and grows unbounded both before and after the unwinding.

3.2 Numerical Methods

For each initial field configuration under investigation the CMB anisotropy is computed in much the same way as in Ref. [28]. For each simulation we follow planes of photons once across the simulation cube, utilising the periodic boundary conditions to allow each plane to travel the same distance through the simulation. The photon planes, each separated by one lattice spacing, are taken to be orthogonal to one of major axes of the cube. We may label each plane by its initial co-ordinate along that axis which corresponds to the label t_i defined above. Following the sheets in sequence then gives the evolution of the anisotropy in time as viewed by the observer. On each plane the temperature is calculated on a grid with the same spacing as the grid for the texture evolution. At each gridpoint at each time step the field's spatial and temporal derivatives are calculated and the integrand of Eq. (16) is summed over the run-time to obtain U . We then calculate $\Delta T/T$ from U using Fast Fourier Transforms.

For configurations admitting an unwinding event 20 photon sheets are chosen such that half pass the unwinding site before the unwinding event occurs and half afterwards. In order to include the necessary post-unwinding field evolution we only consider configurations known to unwind within the first two-thirds of the total run time. Our catalogue of random field configurations [14] contains 11 whose unwinding event meets this criterion, and the specimen spherically symmetric configuration is explicitly chosen so to do. To these we add a further 11 non-unwinding configurations for which we follow all 96 photon sheets. We thus throw out the vast majority of random configurations since only a few percent of such configurations exhibit an unwinding. Our sample therefore has a far greater proportion of unwindings than for patterns picked at random.

4 Results

4.1 CMB Amplitude

As discussed above the SSSS unwinding has a constant CMB anisotropy peak height $\Delta T/T = \pm\epsilon$. As a test of our evolution and CMB anisotropy codes we are able to reproduce this analytic result numerically to within 5%. By comparison the more general spherically symmetric configuration has peak heights

$$\begin{aligned} \frac{\Delta T}{T} \Big|_{\min} &= \begin{cases} -0.56 \epsilon & \text{XCORE} \\ -0.60 \epsilon & \text{NLSM} \end{cases} \\ \frac{\Delta T}{T} \Big|_{\max} &= \begin{cases} +0.67 \epsilon & \text{XCORE} \\ +0.66 \epsilon & \text{NLSM} \end{cases} \end{aligned} \quad (20)$$

Here and subsequently, the asymmetry between the maxima and minima is presumably attributable to the minima being generated earlier in the evolution (photons climbing out of the collapsing texture) than the maxima (photons falling in with the collapsing texture); the field correlations are therefore more pronounced for the maxima systematically enhancing the anisotropy.

Texture field evolution generically includes two sources of metric perturbation. The first is from the collapse, and possible unwinding, of gradient energy on sub-horizon scales, and generates primarily short wavelength modes. The second is from the correlation of the field on horizon scales, and generates primarily long wavelength modes. For spherically symmetric configurations the field is artificially correlated on all scales at the outset, and the second term is not present. However, for random initial conditions this is not the case, and we expect contributions from both sources. The mean peak height associated with the random texture configuration unwinding events is

$$\begin{aligned} \frac{\Delta T}{T} \Big|_{\min} &= \begin{cases} (-0.62 \pm 0.17) \epsilon & \text{XCORE} \\ (-0.66 \pm 0.18) \epsilon & \text{NLSM} \end{cases} \\ \frac{\Delta T}{T} \Big|_{\max} &= \begin{cases} (+0.76 \pm 0.17) \epsilon & \text{XCORE} \\ (+0.78 \pm 0.20) \epsilon & \text{NLSM} \end{cases} \end{aligned} \quad (21)$$

where the error bars here and below are one standard deviation over the set of simulations in question.

We are also interested in the typical amplitude of the background, long wavelength, anisotropy modes. Reading the amplitudes directly from the simulations with no unwinding event is problematic since even here the gradient energy may locally collapse before being annihilated by large scale correlation, introducing short wavelength modes. We find significant non-unwinding events in all but two of the configurations investigated, with over one third of them exhibiting two events. However, none of these occur in events with a true unwinding. The mean anisotropy across each sheet has been set to zero but we can still quantify the amplitude of the long wavelength fluctuations about this by calculating the mean modulus and the standard deviation of the anisotropy averaged over the entire pattern for all simulations. These quantities are measures of the long-wavelength modes since the high peaks which contain most of short-wavelength power subtend a small solid angle. Taking all 22 simulation datasets together we find

$$\begin{aligned} \left| \frac{\Delta T}{T} \right| &= 0.12 \epsilon \\ \sigma &= 0.17 \epsilon \end{aligned} \tag{22}$$

in both the XCORE and NLSM approximations.

The non-unwinding events are of considerable interest, especially in the light of the rarity of actual unwindings. The mean peak anisotropies associated with them are found to be

$$\begin{aligned} \left. \frac{\Delta T}{T} \right|_{\min} &= \begin{cases} (-0.65 \pm 0.29) \epsilon & \text{XCORE} \\ (-0.67 \pm 0.29) \epsilon & \text{NLSM} \end{cases} \\ \left. \frac{\Delta T}{T} \right|_{\max} &= \begin{cases} (+0.60 \pm 0.25) \epsilon & \text{XCORE} \\ (+0.63 \pm 0.25) \epsilon & \text{NLSM} \end{cases} \end{aligned} \tag{23}$$

In order to describe features common to both unwinding and non-unwinding events we shall henceforth use the notion of the event midtime, being the time at which the associated anisotropy changes from being a cold to a hot spot; this is clearly identical to the unwinding time, where one exists. Table 1 provides a quick comparison of the maximum and minimum anisotropies from the different field configurations and numerical methods.

Configuration/Method	$\Delta T/T_{\max}$	$\Delta T/T_{\min}$
SSSS/Analytic	+1	-1
SS/XCORE	0.67	-0.56
SS/NLSM	0.66	-0.60
Random/XCORE	0.76 ± 0.17	-0.62 ± 0.17
Random/NLSM	0.78 ± 0.20	-0.66 ± 0.18
Non-unwinding/XCORE	0.60 ± 0.25	-0.65 ± 0.29
Non-unwinding/NLSM	0.63 ± 0.25	-0.67 ± 0.29

Table 1 Comparison of the peak temperature anisotropies as described in the text. Here SS is the spherically symmetric configuration of Eq. (6) in §2.1. The anisotropies are in units of $\epsilon = 8\pi^2 G\Phi_0^2$.

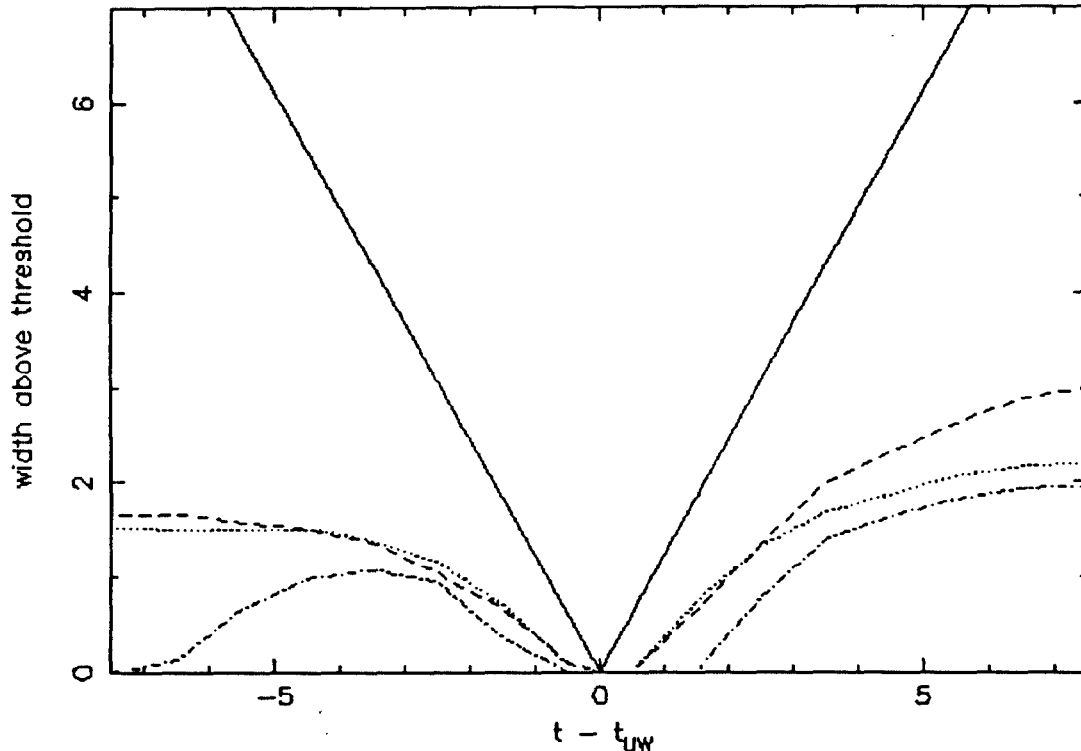


Figure 1 The radii of microwave spots above a given anisotropy threshold, as described in the text. The solid line corresponds to the exact SSSS solution, the dot-dashed to the spherically symmetric simulation, the dashed to the average of the unwinding events and the dotted to the average of the non-unwinding events.

4.2 CMB Spot Size

The size of the CMB spot can be parameterized by the radius at which the anisotropy falls to some specified threshold, $|\Delta T/T| = \xi\epsilon$, at any given time. From Eq. (19) for the SSSS solution this is

$$R_\xi(t_i) = \sqrt{\frac{1 - \xi^2}{2\xi^2}} |t_i| \quad (24)$$

For the more general spherically symmetric configuration we can simply read off the value of the threshold radius from the numerical calculations. In the case of the random configurations the spot radius is calculated by counting all points in the vicinity of the peak with $\Delta T/T \leq -\xi\epsilon$ on sheets whose impact time is before the event's midtime, and with $\Delta T/T \geq +\xi\epsilon$ on those for which it is afterwards, and taking

$$R_\xi(t_i) = \sqrt{\frac{N_\xi(t_i)}{\pi}} \quad (25)$$

where $N_\xi(t_i)$ is the number of lattice points satisfying the appropriate criterion at any impact time. We take the threshold value to be $\xi = 0.5 \epsilon$, being 3σ in the background anisotropy determined above.

Figure 1 shows the variation in mean spot radius with time in each case. In contrast to the linearly divergent SSSS case, in all the other cases the spot radius reaches a maximum

before falling off at early and late times. Except at their midtimes, the random and SS configurations' maximum radii are typically between 1/5 and 1/3 of that of the SSSS solution at the same time.

We would now like to make some estimate of the angular size that these spots would have on the microwave sky. This is never going to be completely satisfactory while we restrict ourselves to flat space simulations, but nevertheless estimates can be made. Recalling our designation of the initial horizon radius as 32 grid units via an estimate of the correlation length, and given that unwindings typically occur after around 30 time units, the horizon radius at unwinding is around 60 grid units. This is to be compared with a typical threshold spot radius of around 3 grid units, so we estimate the spot radius to be of the order of 5% of the horizon radius.

Independent of any simulation parameters, we know directly from cosmology the angle subtended by the horizon at last scattering. As a function of the redshift z of last scattering, it is simply

$$\theta_{\text{hor}} \simeq (1 + z_{\text{ls}})^{-1/2} \text{ radians} \quad (26)$$

The angular radius of the spot on the microwave sky is hence of order

$$\theta_{\xi} \sim \frac{R_{\xi}}{R_{\text{hor}}(t_{\text{uw}})} \theta_{\text{hor}} \quad (27)$$

where $R_{\text{hor}}(t_{\text{uw}})$ is the horizon size at the event's midtime. In the spherically symmetric cases the correlation of the field on super-horizon scales means that the CMB spot may become larger than the horizon away from the unwinding event. This is certainly the case for the SSSS solution, where the spot size grows linearly with impact time, although we note that we would only trust the result Eq. (19) close to the unwinding site. By contrast the general spherically symmetric configuration spot size shows similar behaviour to those of the random configurations, reaching a maximum radius both before and after the midtime. In the SSSS case, since a super-horizon sized coherent anisotropy is unphysical we impose a cutoff at the horizon size, setting the prefactor in Eq. (27) to one, though this is still a far from satisfactory state of affairs suggesting that, at least in estimating metric perturbations in the texture model, one should steer well clear of the SSSS solution whenever possible.

For textures unwinding at decoupling, assuming that these results can be carried into the matter dominated epoch and that the redshift of last scattering is given by one of

$$1 + z_{\text{ls}} \sim \begin{cases} 1000 & \text{no re-ionisation} \\ 50 & \text{re-ionisation} \end{cases} \quad (28)$$

this yields

$$\theta_{\xi} \sim \begin{cases} 0.1^{\circ} & \text{no re-ionisation} \\ 0.4^{\circ} & \text{re-ionisation} \end{cases} \quad (29)$$

Bearing in mind that these are radii, our predicted spot-size appears similar to that found in Ref. [11] who only considered a cosmology with reionisation.

Illustrating these features together, Figures 2a–d shows the spot anisotropy profile for the SSSS solution, the spherically symmetric configuration, a typical unwinding event and a typical non-unwinding event. In each case the profiles are taken immediately before, at, and immediately after the midtime.

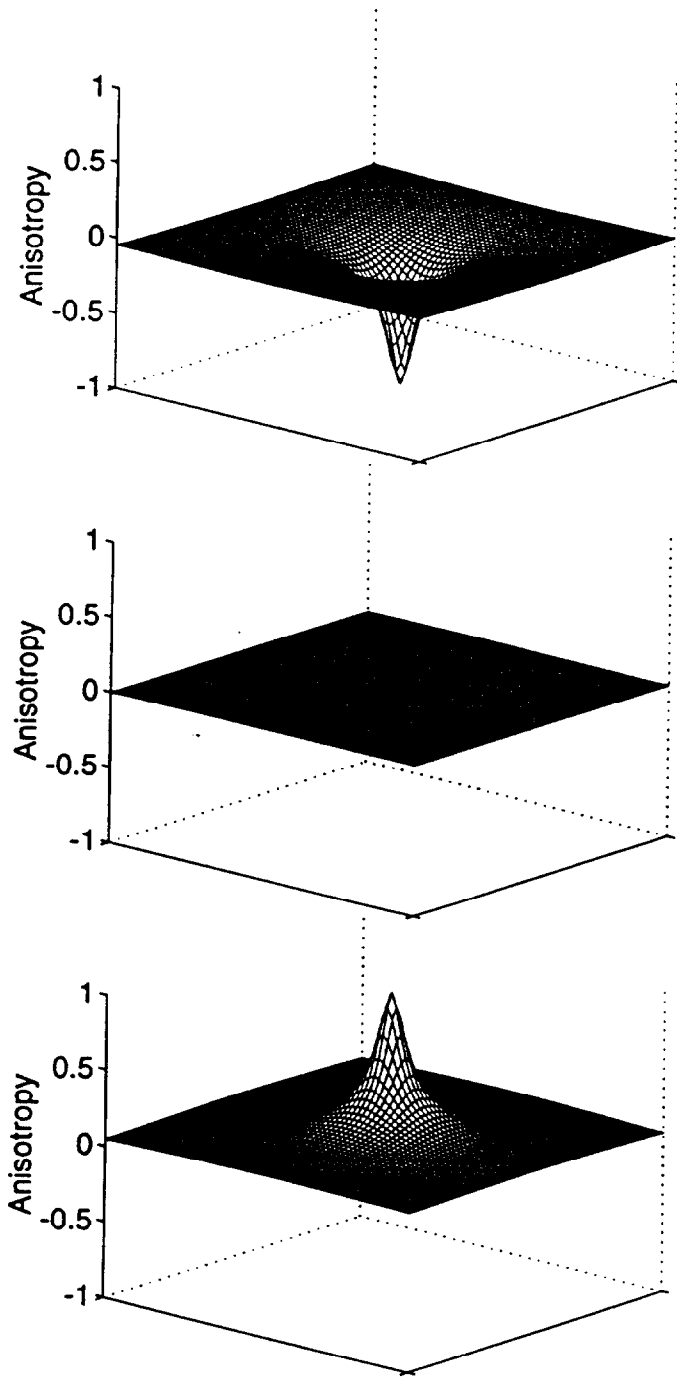


Figure 2a The fractional anisotropy generated by the evolution of various initial field configurations in units of ϵ . In each case three photon sheets are shown, being three gridtimes before, at, and three gridtimes after the event midtime. These are (a) the SSSS exact solution,

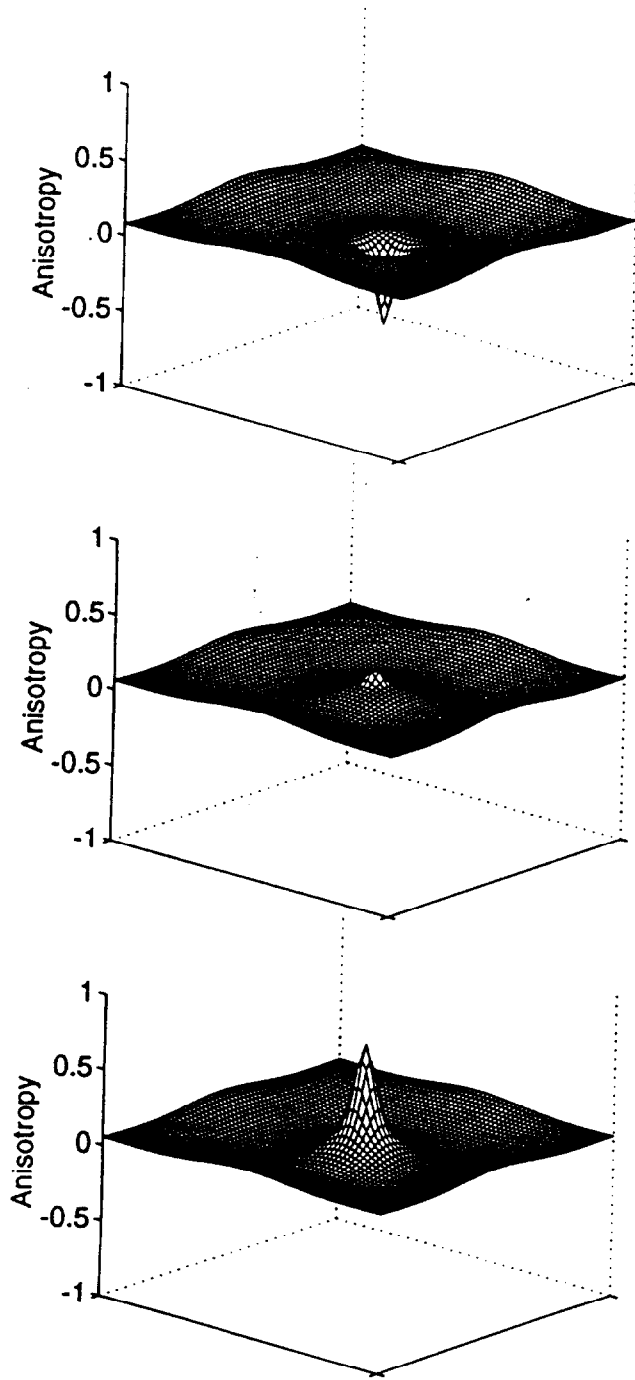


Figure 2b (b) the spherically symmetric configuration,

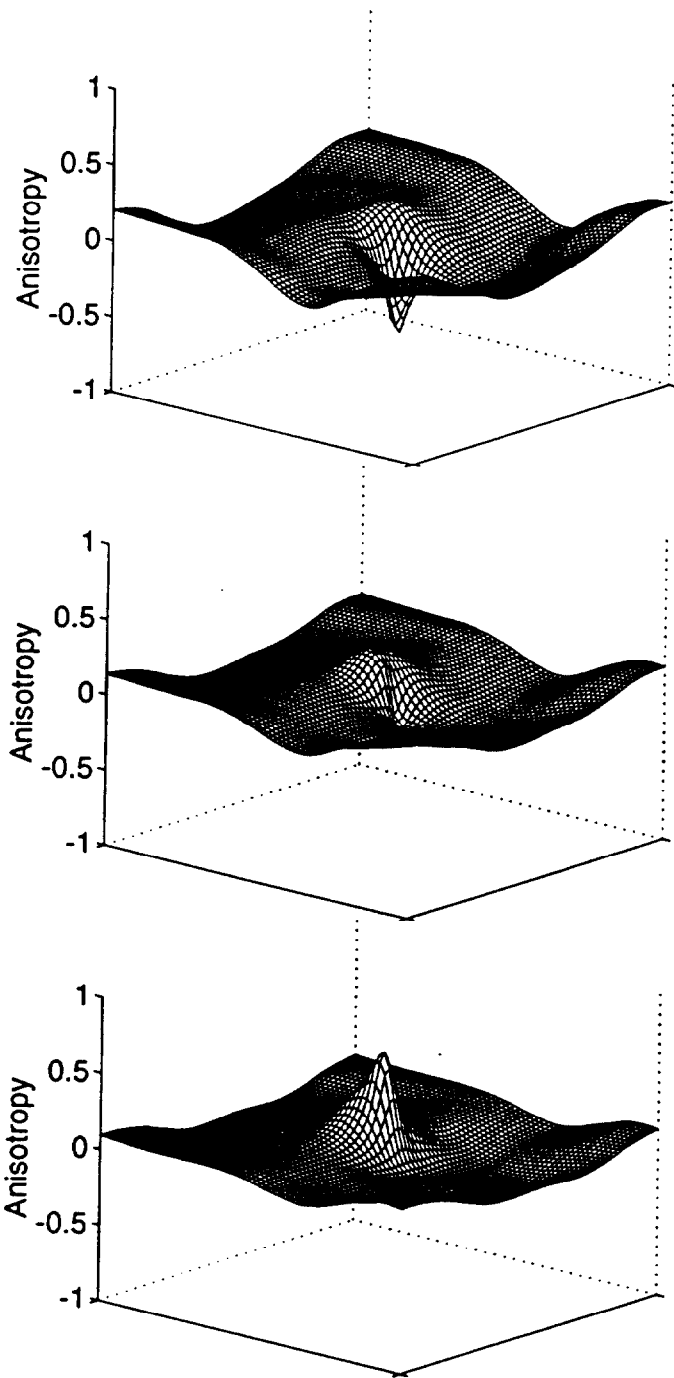


Figure 2c (c) a typical random unwinding configuration,

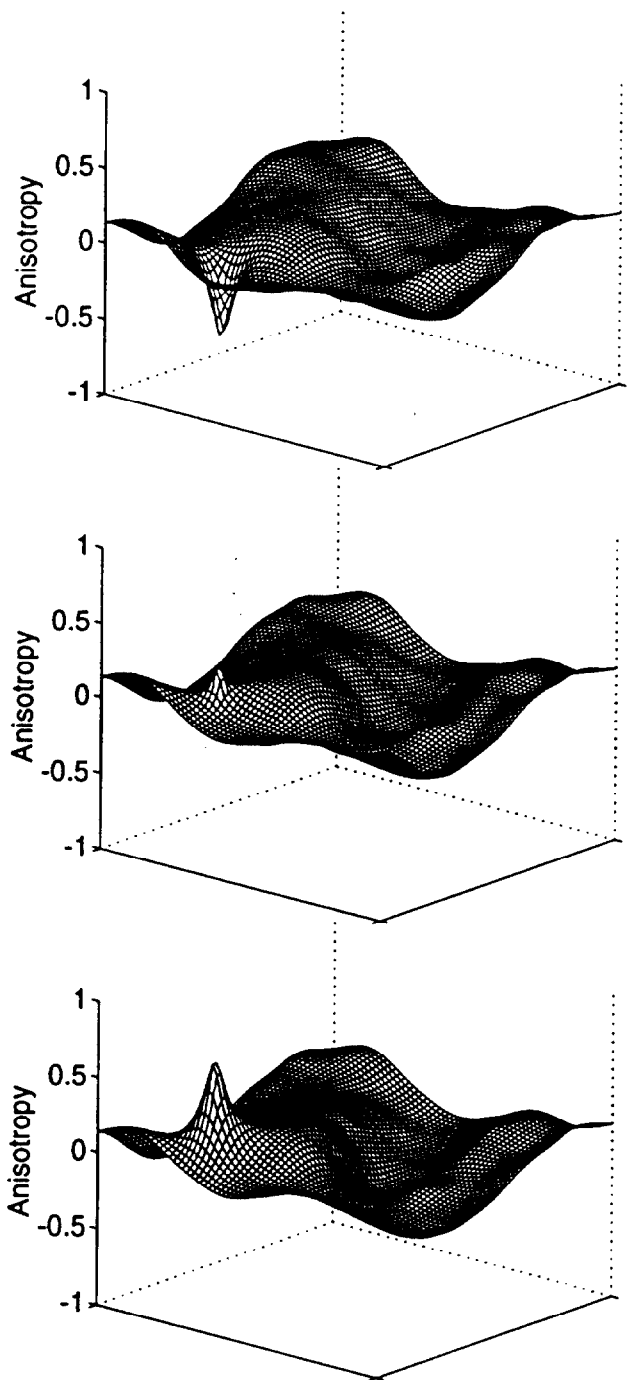


Figure 2d and (d) a typical random non-unwinding configuration.

5 Discussion

It is encouraging to note the strong consistency between the results in the XCORE and NLSM approximations. Not only can the statistical results over the ensemble of simulations be treated as identical, but individual simulations with the same initial conditions exhibit events whose individual properties are quantitatively extremely similar. Since the two approximation methods are very different, this congruence of results lends considerable weight to our belief that both sets of simulations are accurately modelling the texture field's evolution. While this is only the case at the level of resolution employed here (in both approximations any significant reduction in resolution is seen to introduce serious numerical errors — see Ref. [18] for details), we are confident that the results in this paper are trustworthy and allow a genuine comparison between numerical calculations and the analytic solutions.

Our key results from this comparative study are the following

1. The randomly generated configurations produce microwave anisotropy patterns with completely different properties to the exact NLSM solution.
2. Localised concentrations of gradient energy which do *not* lead to unwindings can still generate anisotropies which are extremely similar to those generated by genuine unwindings.
3. We find a characteristic spot size considerably smaller than the horizon size at the collapse time.

Let us comment on each of these in turn, before making some final comments on the relation between our work and that of other authors.

We have found considerable differences between the properties of the microwave anisotropies generated by the exact SSSS solution and our more realistic randomly generated configurations. The peak anisotropy of the random configurations is smaller by 20–40%, and much more significantly the spot size is considerably smaller, leading to a huge reduction in the spot area on the sky and hence in the anisotropy integrated over a beam profile. This effect can doubtless be attributed to the SSSS configuration's spherical symmetry imposing unphysical correlations on scales vastly greater than the horizon size whilst its self-similarity forces the collapse to occur as fast as causally possible, together leading to a maximisation of the anisotropies. The failure of the SSSS solution to represent the properties of true textures appears to be even more dramatic when looking at microwave anisotropies than the failure already noted [13, 14] when only considering the unwinding dynamics.

Perhaps our most significant result is the observation that localised concentrations of gradient energy which nevertheless fail to unwind can still lead to very substantial microwave anisotropies; indeed the anisotropies due to such non-unwinding events are indistinguishable from those due to unwinding events. Furthermore the number density of such events is vastly greater than that of unwinding events; unwinding events occur only in around 4% of our simulations whilst non-unwinding events typically occur once per simulation. Given their indistinguishability we are led to believe that the non-unwinding events are the dominant contributors to the microwave background anisotropies, with unwinding events playing only a minor role.

Our estimate of the spot size is that their typical radius is around 5% of the horizon radius at the time the spot is generated. As stated above, this is considerably smaller than that

generated by the SSSS solution, although that solution can only have a spot size attributed at all by the imposition of a horizon-size cut-off to remove the unphysical correlations. If we follow most authors in assuming that the texture scenario re-ionises the universe to a redshift of around 50, and take the liberty of extrapolating our flat space results directly into a matter dominated universe, then we anticipate a typical spot diameter, be it generated by an unwinding or a non-unwinding event, of about a degree. By contrast, in the absence of re-ionisation the typical spot diameter is only of the order of 10 arcminutes.

Our study has been entirely a comparative one, concentrating on the relative results from alternative choices of initial conditions and approximation methods in the simplest possible environment. The emphasis has been primarily focussed on the behaviour of individual textures. We have not attempted any full cosmological simulations, and indeed the computing resources which we believe are required to mount accurate simulations of ensembles of textures are beyond those available at present (see Refs. [22, 18] for a detailed discussion). The cosmological simulations that have been done [10, 11, 5] may therefore include systematic errors due to their inability sufficiently to resolve the microphysical events associated with the concentration of field gradient energy. In particular it should be noted that low resolution simulations are susceptible to spurious unwinding events, where configurations covering less than half of the vacuum manifold nonetheless unwind. With this caveat firmly in mind we now compare our results with those from such simulations.

The most interesting paper to consider in this context is that of Coulson *et al* [11], who include a large number of physical processes in their cosmological NLSM simulations in an attempt to generate predictions for degree scale anisotropies. We are unable to say anything about their quantitative value for the magnitude of the anisotropy, or even about the statistics, as we have no guidance as to how to combine our different choices of initial conditions into an ensemble. Nevertheless, in two important *qualitative* aspects we are in good agreement with their results. Firstly, their spot size is typically of order one to two degrees (it is slightly hard to estimate which as they smooth their data with a gaussian filter on around this scale). This is considerably less than the horizon size as they assume re-ionisation, and hence is in conflict with the original expectation based on the NLSM solution that the spots would be of order ten degrees [7, 8]. However it is consistent with our result that typical texture unwindings do not lead to such large spots. Secondly, they exhibit a diagram of their simulation covering an area thirty degrees on a side (i.e. about 2% of the sky) which includes several spots. However, the number density of texture unwindings is known to be so low [3, 22] that it is very unlikely that even a single unwinding would have occurred in such an area. It is possible therefore that their spots actually correspond to non-unwinding events, which we have seen greatly dominate over unwinding events while giving rise to a very similar signature, although such results would also be consistent with spurious unwinding events. Qualitatively therefore our picture of many small spots is consistent with their results, although we emphasise again that we have no means of assessing their quantitative estimates.

However, our results do seriously undermine the alternative method of estimating microwave background anisotropies, where photons are traced through an ensemble of SSSS initial configurations which are evolved in flat or matter-dominated backgrounds [8]. The spots found in such calculations are probably too bright by a modest factor, but much more significantly the area is overestimated by a factor which could easily be in the range 25–100 — both factors being attributable to the use of a maximal coherent initial velocity field. On the other hand such simulations only include unwinding events, whereas in practice the

all-sky anisotropy is dominated by non-unwinding events, so the number of spots appearing in their simulations is down, conceivably by a similar factor. Such opposing effects may enable simple measures such as the all-sky rms fluctuation to emerge in acceptable agreement with other derivations (e. g. Ref. [10]), despite the detailed microwave anisotropy distribution being totally different.

Acknowledgements

JB and EJC are supported by the SERC, ARL by the SERC and the Royal Society, AS by the DOE and NASA grant NAGW-2381 at Fermilab and SVR by the NRC. EJC, ARL, AS and SVR would like to thank the Aspen Center for Physics for their hospitality while part of this work was done. We thank Mark Hindmarsh for helpful discussions. ARL acknowledges the use of the STARLINK computer system at the University of Sussex.

References

- [1] E. W. Kolb and M. S. Turner, *The Early Universe*, Addison-Wesley (1990).
A. R. Liddle and D. H. Lyth, *Phys. Rep.* 231, 1 (1993).
- [2] T. W. B. Kibble, *J. Phys. A* **9**, 1387 (1976).
- [3] N. Turok, *Phys. Rev. Lett.* **63**, 2625 (1989).
- [4] A. Vilenkin, *Phys. Rep.* 121, 263 (1985).
- [5] D. P. Bennett and S. H. Rhie, *Phys. Rev. Lett.* **65**, 1709 (1990).
- [6] R. Y. Cen, J. P. Ostriker, D. Spergel and N. Turok, *Astrophys. J.* **383**, 1 (1991).
A. K. Gooding, C. Park, D. Spergel, N. Turok and J. R. Gott, *Astrophys J* **393**, 42 (1992).
- [7] N. Turok and D. N. Spergel, *Phys. Rev. Lett.* **64**, 2736 (1990).
- [8] R. Durrer and D. N. Spergel, in "Trends in Astroparticle Physics" ed. D Cline & R. Peccei, World Scientific (Singapore) (1992).
R. Durrer, A. Howard and Z-H Zhou, *Phys. Rev. D* **49**, 681 (1994).
- [9] D. P. Bennett and S. H. Rhie, *Astrophys. J. Lett.* **406**, L7 (1993).
- [10] U.-L. Pen, D. N. Spergel and N. Turok, *Phys. Rev. D* **49**, 692 (1994).
- [11] D. Coulson, P. Ferreira, P. Graham and N. Turok, "Microwave Anisotropies from Cosmic Defects", *Nature*, in press (1994).
- [12] G. F. Smoot *et al*, *Astrophys. J. Lett.* **396**, L1 (1992).
- [13] J. Borrill, E. J. Copeland and A. R. Liddle, *Phys. Rev. D* **46**, 524 (1992).
- [14] J. Borrill, E. J. Copeland and A. R. Liddle, *Phys. Rev. D* **47**, 4292 (1993).
- [15] M. Nagasawa, K. Sato and J. Yokoyama, *Publ. Astron. Soc. Japan* **45**, 755 (1993).

- [16] S. Veeraraghavan and A. Stebbins, *Astrophys. J.* **365**, 37 (1990).
- [17] S. Veeraraghavan and A. Stebbins, *Astrophys. J. Lett.* **395**, L55 (1992).
A. Stebbins and S. Veeraraghavan, *Phys. Rev. D***48**, 2421 (1993).
- [18] J. Borrill, "Numerical Methods in Cosmological Global Texture Simulations", Imperial College preprint IMPERIAL/TP/93-94/22 (1994).
- [19] W. H. Press, B. P. Flannery, S. A. Teukolsky and W. T. Vetterling, *Numerical Recipes* (Cambridge University Press 1986)
- [20] W. H. Press, B. S. Ryden and D. N. Spergel, *Astrophys. J.* **347**, 590 (1989).
- [21] D. N. Spergel, N. Turok, W. H. Press and B. S. Ryden, *Phys. Rev. D***43**, 1038 (1991).
- [22] J. Borrill, *Phys. Rev. D***47**, 4298 (1993).
- [23] R. Sachs and A. Wolfe, *Astrophys. J.* **147**, 73 (1967).
- [24] A. Stebbins, *Astrophys. J.*, **327**, 584 (1988).
- [25] M. Hindmarsh, "Small Scale Microwave Background Fluctuations from Cosmic Strings", *Astrophys. J.*, in press (1994).
- [26] S. Veeraraghavan and A. Stebbins, "Beyond the Small Angle Approximation for MBR Anisotropy from Seeds", Fermilab preprint Fermilab-Pub-94/047-A (1994).
- [27] S. Veeraraghavan and A. Stebbins, in preparation (1994).
- [28] F. Bouchet, D. Bennett and A. Stebbins, *Nature* **335**, 410 (1989).